PHYSICAL REVIEW B VOLUME 36, NUMBER 10 1 OCTOBER 1987

Magnetic behavior of the diluted magnetic semiconductor $(Zn_{1-x}Mn_x)_3As_2$

C. J. M. Denissen, Sun Dakun,* K. Kopinga, and W. J. M. de Jonge
Department of Physics, Eindhoven University of Technology, P.O. Box 513, 5600 MB Eindhoven, The Netherlands

H. Nishihara, T. Sakakibara, and T. Goto
Institute for Solid State Physics, University of Tokyo, Roppongi 7, Tokyo 106, Japan
(Received 8 October 1986)

$(Zn_{1-x}Mn_x)_3As_2$, abbreviated as ZMA, can be considered as a new member of the group of diluted magnetic semiconductors (DMS). Susceptibility and specific-heat measurements indicate a spin-glass transition for concentrations $0.005 < x < 0.14$. The freezing temperature T_f depends on x as $T_f \sim x^{1.5}$, originating from a long-range interaction J between magnetic ions $J(R) \sim R^{-4.5}$. High-field magnetization and high-temperature susceptibility measurements yield evidence for an overall antiferromagnetic interaction, a strong antiferromagnetic coupling of nearest-neighbor Mn pairs, and a reduced (20%) local moment of the Mn ions. Calculations of M, χ, and C_m with an extended nearest-neighbor pair-correlation approximation will be reported. A satisfactory, simultaneous description of the data can be obtained, providing the long-range character of the exchange is properly taken into account. The results will be compared with other DMS and recently prepared quaternary alloys of $(Cd_{1-y-x}Zn_yMn_x)_3As_2$. Possible mechanisms for the interaction will be discussed.

I. INTRODUCTION

$(Zn_{1-x}Mn_x)_3As_2$, abbreviated ZMA, can be considered as a solid solution of the open-gap semiconductor Zn_3As_2 and Mn_3As_2. Together with $(Cd_{1-x}Mn_x)_3As_2$ (CMA) (Ref. 1) this compound belongs to the II-V group of diluted magnetic semiconductors (DMS). The crystal structure of ZMA is isomorphic with that of CMA (tetragonal, $P4_2/nmc$), but the lattice constants are somewhat smaller.[2]

One of the interesting problems in the study of the magnetic properties of DMS concerns the physical mechanism behind the interactions between the Mn ions. In an earlier publication[1] we introduced and discussed already some possible physical mechanisms in relation to our results obtained in CMA. Tentatively we reached the conclusion that, in CMA, two possible interaction mechanisms were compatible with the results: the Bloembergen-Rowland and the superexchange mechanism. In the Bloembergen-Rowland mechanism the gap between conduction and valence band determines the range of the interaction. ZMA is an open-gap semiconductor ($\varepsilon_0 \simeq 1$ eV),[2] whereas CMA is a narrow-gap semiconductor ($\varepsilon_0 \simeq -0.1$ eV). In view of this difference in band gaps, it seemed worthwhile to study also the magnetic properties of ZMA, since these may yield additional information on the interaction mechanism.

Data will be presented on specific heat, low- and high-temperature susceptibility, and magnetization. The observed spin-glass freezing as function of concentration will be used as a probe for the long-range part of the interaction, which has to be implemented to obtain a set of interaction parameters which, in principle, can describe all the data simultaneously.

The experiments were performed on a number of samples with Mn^{2+} concentrations in the range $0.005 < x < 0.14$ (see Table I). The experimental methods and equipments are identical to those applied in the study of CMA, and we refer to that article for details.[1]

$(Zn_{1-x}Mn_x)_3As_2$ (ZMA) was grown by a modified Bridgman method from the pure elements in a carbon-coated ampoule (pressure 10^{-5} mbar). The ampoules were heated up till 1100 °C, which is above the melting point of Zn_3As_2 (1015 °C).[2] The pulling speed was 20 mm/day. In this way we obtained single phase crystals up to $x \simeq 0.15$, the highest concentration we tried to grow. Often large single crystals with a typical volume of 0.5–1 cm^3 were obtained. For most experiments, such as calorimetry, susceptibility, and magnetization, polycrystalline samples are appropriate. A single-crystal of ZMA, $x = 0.15$, with a volume of more than 1 cm^3, was grown especially for use in neutron scattering experiments in the near future.

For the interpretation of the experimental results, the chemical and structural definition of the samples is sometimes of crucial importance. X-ray diffraction, electron microprobe measurements and chemical analyses were employed to ensure a proper characterization of the samples. A homogeneous composition without chemical clustering has been found, within the limits of the techniques employed (1 μm). Generally, the measured concentrations x varied slightly over the samples and the relative accuracy of the Mn concentration was better than 10%.

II. EXPERIMENTAL RESULTS

A. Low-temperature ac susceptibility

The low temperature ac susceptibility results for ZMA are shown in Fig. 1. For all concentrations 0.005

TABLE I. Composition of the relevant samples $(Zn_{1-x}Mn_x)_3As_2$ used in the present experiments.

Sample no.	x (nominal)	Large sample $\bar{x}$ (specific heat)	Small sample $\bar{x}$ (susceptibility + magnetization)
0.5 ZMA-1	0.005	0.0052	0.0048
			0.0052
1 ZMA-1	0.01	0.0104	0.010
			0.010
3 ZMA-1	0.03	0.03	0.030
			0.031
5 ZMA-1	0.05	0.049	0.049
			0.049
7 ZMA-1	0.07		0.066
10 ZMA-1	0.10	0.098	0.098
			0.097
12 ZMA-1	0.12		0.112
15 ZMA-1	0.15		0.14
15 ZMA-1 (single crystal)	0.15	0.14	

$<x<0.14$ cusps in $\chi(T)$ are observed, whereas, as we will see later on, no anomalies occur in the specific heat. Interpreting these cusps as a transition to a spin-glass state, the resulting freezing temperatures $T_f(x)$ are shown in Table II. From a plot of $\log T_f$ against $\log x$, shown in Fig. 2, it appears that $T_f(x)$ behaves approximately as $T_f(x)\sim x^{3/2}$ over the entire concentration range. As we observed the spin-glass transition below the percolation limit for nearest neighbors, which amounts to 33% in this case, one may already conclude that the interactions are long ranged. Moreover, according to scaling arguments[3,4] a dependence $T_f\sim x^{3/2}$ can be related to a long-range exchange of the type $J\sim R^{-9/2}$, where R is the distance between the magnetic ions. The results on $T_f(x)$ of CMA are also shown in Fig. 2. It is obvious that the interaction in CMA $(J\sim R^{-7/2})$ is of slightly longer range than that in ZMA.

B. Specific heat in zero field

The magnetic contribution C_m to the specific heat in the range $0.4<T<8$ K (as shown in Fig. 3) was obtained by subtraction of the (scaled) lattice contribution of pure Zn_3As_2 (Fig. 4) and the nuclear hyperfine contribution of the Mn-ions[5] from the measured total specific heat. As already quoted above, no anomaly was observed at temperatures $T_f(x)$, which are indicated by arrows in the figure. The overall contribution shows the conventional broad maximum, typically for a nonordering ensemble of interacting spins. The location of the maximum, which is a measure for the magnitude of the average interaction energy, shifts systematically to higher temperatures (from 0.5 K to above 6 K) as the concentration increases from 1 to 10 at. %. This fact also points to a long-range interaction. A model with

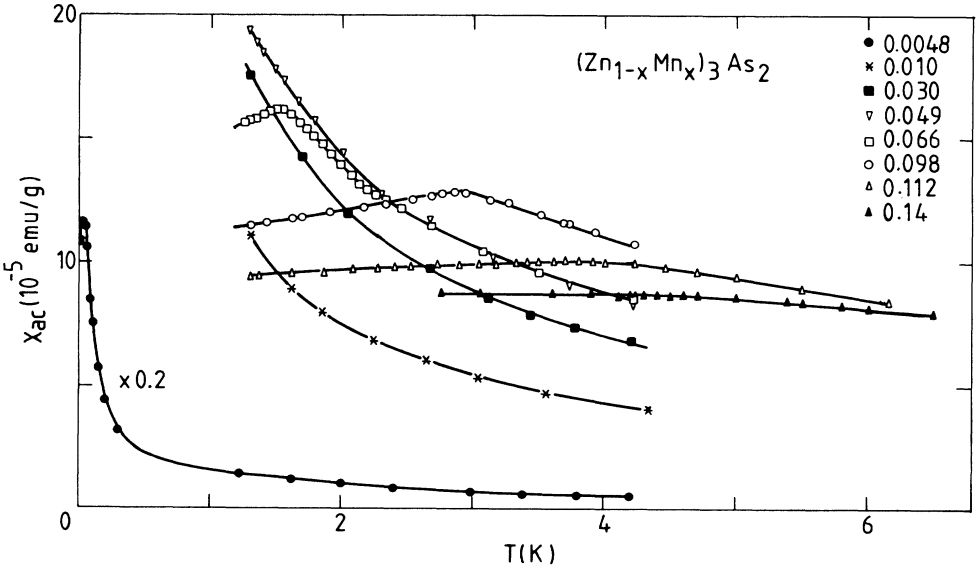

FIG. 1. Low-temperature ac susceptibility of ZMA. The solid curves are guides to the eye.

TABLE II. Freezing temperature of ZMA as a function of the Mn concentration.

x	T_f (K)
0.0048	0.035
0.03	0.7
0.066	1.55
0.098	2.85
0.112	3.6
0.14	4.3

only nearest- and next-nearest-neighbor interactions cannot account for this behavior. We will return to this subject in the discussion.

C. Magnetization

Magnetization experiments were performed in the field range up to 28 T and the temperature range $2 < T < 4.2$ K. The results are shown in Fig. 5.

From a comparison of the behavior with that of an ideal paramagnetic gas it can be concluded that the average interaction must be antiferromagnetic. Furthermore, an increase of concentration yields an obvious increase of the average interaction strength. Saturation in the present field range is achieved for concentrations up to 1 at. %.

The magnetization curves can be fitted with the phenomenological Brillouin function

$$M = g\mu_B S_0 B_{5/2}\left[\frac{2.5 g\mu_B B}{k_B T_{\text{eff}}}\right], \tag{1}$$

where the (apparent) saturation magnetization per Mn ion, $g\mu_B S_0$, and the effective temperature, $T_{\text{eff}} = T + T_0$, are adjustable. These fits are also shown in Fig. 5. The resulting values of gS_0 and T_0 are given in Table III.

The saturation magnetization per ion $g\mu_B S_0$ is plotted

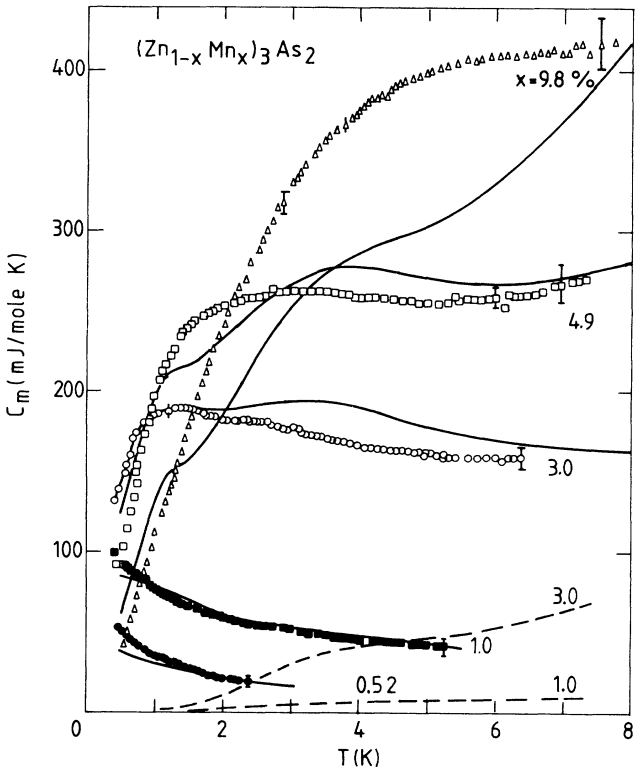

FIG. 3. Magnetic specific heat of ZMA. The arrows indicate the freezing temperatures T_f for the corresponding concentrations. The solid curves represent calculations with the ENNPA using $J_1/k_B = -100$ K, $J_2/k_B = -20$ K, $J_3/k_B = -6$ K, and $J/k_B = -40/R^{4.5}$ K. The dashed curves represent calculations with the ENNPA using the same values for J_1, J_2, and J_3 as above but $J/k_B = 0$ K.

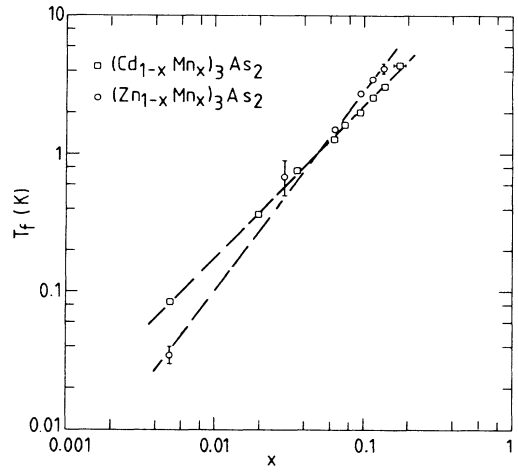

FIG. 2. Log T_f-log$x$ plot for ZMA and CMA. The dashed curves represent $T_f \sim x^{3/2}$ and $T_f \sim x^{7/6}$, respectively.

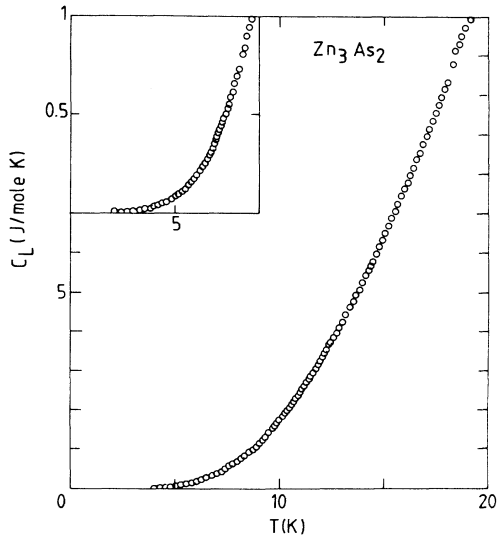

FIG. 4. Specific heat of Zn_3As_2.

TABLE III. Saturation magnetization per ion gS_0 of ZMA and temperature T_0 obtained from a fit of the magnetization to an effective Brillouin function.

x (at. %)	gS_0	T_0 (K)
0.52	3.9	1.8
1.0	3.5	3.0
3.0	2.5	9
4.9	1.9	12
9.7	1.2	18

in Fig. 6 as function of x, supplemented with the extrapolated results based on fits of the data to a phenomenological Brillouin function for concentrations $x > 0.01$. These results show that, in the limit of vanishingly small concentrations of magnetic ions, the saturation magnetization per ion $g\mu_B S_0$ approaches the value of $(4.1 \pm 0.2)\mu_B$ instead of the value of $5\mu_B$ for a Mn^{2+} ion in the S state. Susceptibility results, which will be discussed below, support this conclusion. A similar reduction of the free-ion moment was found in CMA.[1] We will comment on this fact in the discussion.

Apart from this, the measured saturation value decreases when the concentration increases. In CMA this reduction was caused by strongly coupled antiferromagnetic pairs, which did not contribute to the magnetization in fields up to 28 T. However, in the case of ZMA the observed reduction of the saturation magnetization cannot be explained with the pairing of nearest neighbors alone. Therefore we calculated the theoretical saturation magnetization under the assumption that the nearest- and next-nearest-neighbor pairs do not contribute in this field range, because they are strongly coupled antiferromagnetically. The predicted moment as function of x is shown in Fig. 6. The fractions of singles,

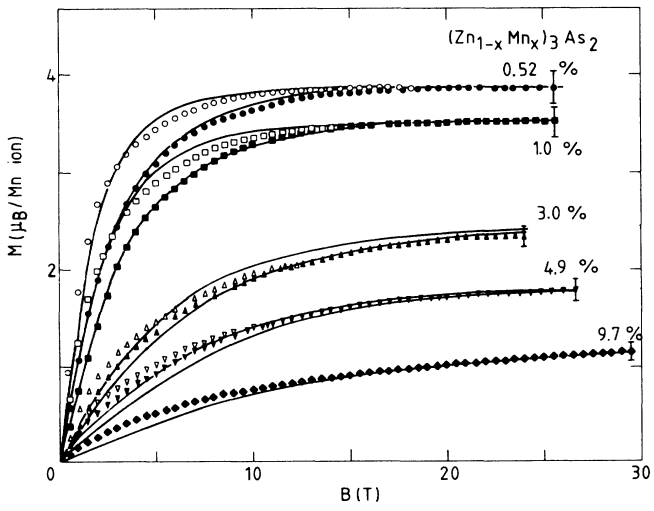

FIG. 5. High-field magnetization of ZMA for selected concentrations. Open and closed symbols represent data collected at $T=2$ K and $T=4.2$ K, respectively. The solid curves represent fits with the phenomenological Brillouin function.

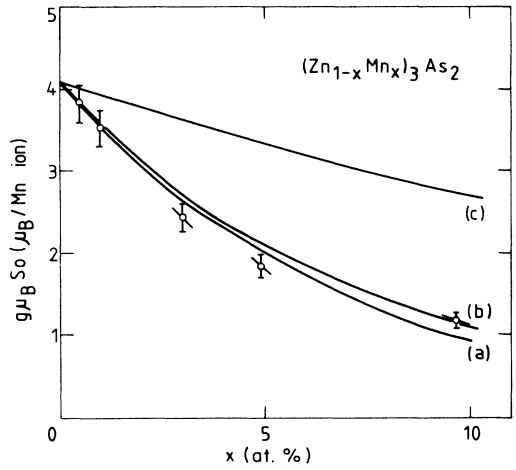

FIG. 6. Saturation magnetization per Mn ion, $g\mu_B S_0$, as a function of x of ZMA. Curve a represents the contribution of the statistical fraction of singles (no nearest and next-nearest neighbors) to the saturation. Curve b includes also the contribution of $\frac{1}{3}$ of the statistical fraction of open triples (nearest and next-nearest neighbors). Curve c represents the contribution of the singles with respect to only nearest neighbors.

pairs, and triples have been obtained from a random distribution of Mn ions. Comparison of the actual data with this prediction shows a very good agreement, although we have to recall that the data at high x are extrapolated results.

Since we do not observe any decoupling in fields up till 28 T, which would lead to a "steplike" increase of the magnetization, the antiferromagnetic nearest- and next-nearest-neighbor coupling energy in ZMA seems to amount to at least 40 K or, alternatively, $|J_1/k_B|$ and $|J_2/k_B|$ are larger than 20 K.

D. High-temperature susceptibility

Magnetization measurements in various fields up to 1.2 T yielded a linear behavior for temperatures above 4.2 K. Susceptibility measurements were performed for $4.2 < T < 300$ K in a static magnetic field $B = 1.2$ T with a pendulum method. The data corrected for the diamagnetic contribution of Zn_3As_2, which was obtained separately as -2×10^{-7} emu/g are shown in Fig. 7. (Strictly speaking, the units for mass susceptibility are erg $G^{-2}g^{-1}$. However, for the sake of convenience, we use emu/g.) At sufficiently high temperatures the data appear to follow a Curie-Weiss behavior given by

$$\chi - \chi_0 = C/(T-\Theta) , \tag{2}$$

where Θ is the Curie-Weiss temperature. The slope of the plots of $1/(\chi-\chi_0)$ against T is determined by the factor $C = 3xNg^2\mu_B^2 S(S+1)/3k_B M$, where N is Avogadro's number and M the molar weight.

The resulting values for $g[S(S+1)]^{1/2}$ and gS (assuming $g=2$) are given in Table IV. As we already anticipated from the high-field magnetization data, the moment appears to be reduced $[(4.4\pm0.2)\mu_B]$ with respect

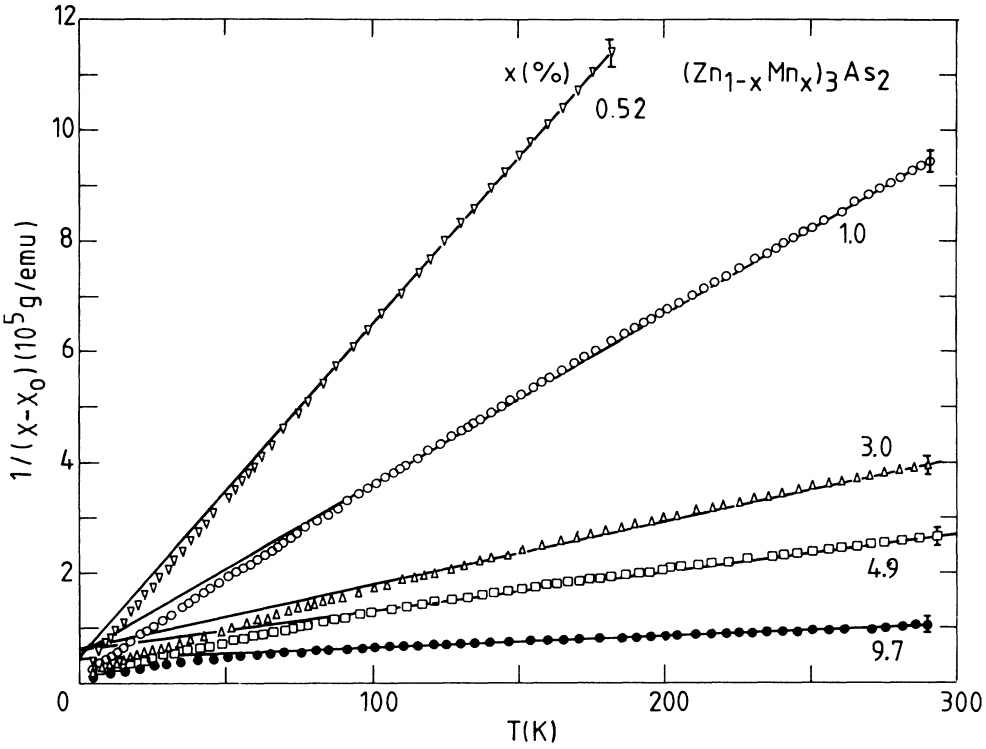

FIG. 7. Inverse high-temperature susceptibility of ZMA. The solid lines represent the limiting high-temperature Curie-Weiss behavior.

to the free-ion value ($5\mu_B$). The somewhat deviating moment obtained for the highest concentration may be due to the fact that for this concentration the temperature region at which the experiments are performed is not sufficiently high to observed Curie-Weiss behavior.[6]

For all concentrations x, the Curie-Weiss temperature Θ is negative (antiferromagnetic) and is proportional to x, as plotted in Fig. 8. It is important to note that these high-temperature data (or more specifically Θ) contain all the interactions, in contrast to the magnetization and specific-heat data, where the strong antiferromagnetic nearest- and next-nearest-neighbor interactions eliminate the contribution of the pairs and triples.

Using a high-temperature series expansion (HTSE), a model in which the localized magnetic moments are subjected to a nearest-neighbor exchange J_1, a next-nearest-neighbor exchange J_2, etc., supplemented with a long-range interaction of the type $J(R)=JR^{-9/2}$ for further neighbors, yields

$$\Theta=\frac{2S(S+1)x}{3k_B}\left[\sum_1^n N_iJ_i+\sum_n^\infty N_jJR_j^{-9/2}\right], \tag{3}$$

where N_i is the number of neighbors coupled by J_i and

TABLE IV. Magnetic moment (or spin) of ZMA resulting from the high-temperature susceptibility.

x (at. %)	$g[S(S+1)]^{1/2}$	gS $(g=2)$
0.52	5.4	4.5
1.0	5.5	4.6
3.0	5.1	4.2
4.9	5.1	4.2
9.7	6.6	5.6

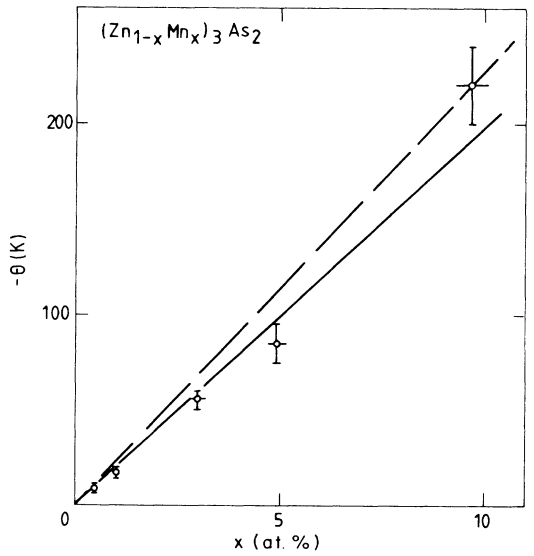

FIG. 8. Curie-Weiss temperature Θ as a function of x. The solid line represents the best fit $\Theta=-(2000\pm200)x$ K. The dashed line results from Eq. (9), with the interaction parameters obtained from the ENNPA.

N_j is the number of neighbors at the distance R_j (R_j is in units of the nearest-neighbor distance, $R_1 \equiv 1$).

Confronting this expression with the experimentally observed behavior $\Theta(x) = -(2000 \pm 200)x$ K yields a relation between the strength of the interaction parameters. It is also worthwhile to note that the experimentally observed linear behavior of $\Theta(x)$, as well as the fact that all fits to the high-temperature susceptibility data intersect at $T = 0$, are in complete agreement with Eqs. (3). This observation therefore corroborates the basic assumption about the random distribution of the magnetic ions, on which Eq. (3) is based.

III. INTERPRETATION

Inspection of the experimental zero field specific heat, the magnetization and the susceptibility data has shown that these results can—at least qualitatively—be understood on the basis of the following assumptions:

(i) Relatively strong antiferromagnetic (AF) nearest- and next-nearest-neighbor interactions J_1 and J_2.

(ii) An AF long-range interaction of the type $JR^{-9/2}$.

(iii) A random distribution of Mn ions.

(iv) $gS \simeq 4.3$, the average between magnetization and susceptibility results (or, since we like to use "real" spin values, $g = 2.15$ and $S = 2$).

This physical model is quite similar to the model used for the interpretation of the results on CMA. For the calculations of the relevant thermodynamic properties from this model we used an extended version of the pair approximation model [extended nearest-neighbor pair approximation(ENNPA)]. This approximative calculation method is particularly useful for random arrays with long-range interactions. It has been introduced by Matho[7] for canonical metallic spin glasses and has also been successfully applied to diluted magnetic semiconductors.[8] The approximation basically rests on the assumption that the partition function of the system can be factorized into contributions of pairs of spins. Each spin is considered to be coupled with an exchange J_ν only to its nearest *magnetic* neighbor, located at a distance R_ν from the reference site; the population of magnetic ions in the shells R_ν is determined assuming a random distribution of these ions. The model is extended with respect to the original suggestion of Matho[7] with exchange coupled triples, i.e., configurations in which two spins are located at the same distance from the reference spin. The Hamiltonians for a pair and a triple are given by

$$\mathcal{H}_\nu^P = -2J_\nu \mathbf{S}_i \cdot \mathbf{S}_\nu - g\mu_B (S_i^z + S_\nu^z) B^z , \tag{4}$$

$$\mathcal{H}_\nu^T = -2J_\nu \mathbf{S}_i \mathbf{S}_{\nu,1} - 2J_\nu \mathbf{S}_i \cdot \mathbf{S}_{\nu,2} - g\mu_B (S_i^z + S_{\nu,1}^z + S_{\nu,2}^z) B^z , \tag{5}$$

where $J_\nu = f(R_\nu)$. N_ν is the number of lattice sites in shell ν. Using $n_\nu = \sum_1^\nu N_\nu$ for $\nu > 0$ and $n_0 = 0$, the probability of finding the nearest spin in the νth shell, for a random distribution of spins is

$$P_\nu(x) = (1-x)^{n_{\nu-1}} - (1-x)^{n_\nu} . \tag{6}$$

The probability of finding two neighbors in the same shell (triple) is

$$P_\nu^T(x) = \tfrac{1}{2} N_\nu (N_\nu - 1) x^2 (1-x)^{n_\nu - 2} . \tag{7}$$

The probability for a pair is taken as

$$P_\nu^P(x) = P_\nu(x) - P_\nu^T(x) . \tag{8}$$

The total free energy and other thermodynamic properties can be obtained by summing the respective contributions over the shells ν according to the probability of the pairs and triples in shell ν. J_ν is determined by the range of the magnetic interaction $J_\nu = f(R_\nu)$. R_ν is in units of the nearest-neighbor distance. The summation over the shells ν is carried out up to shell $\bar{\nu}$ for which $\sum_{\nu=1}^{\bar{\nu}} (P_\nu^P(x) + P_\nu^T(x)) \geq 99.5\%$.

In the process of fitting the exchange parameters it was found necessary to treat also J_3 (the third-nearest-neighbor interaction) as an adjustable parameter. The interactions are then J_1, J_2, J_3, and $J_\nu = JR_\nu^{-9/2}$ for $\nu > 3$, where R_ν is in units of the nearest-neighbor distance ($R_1 \equiv 1$). The results of the calculations are shown in Figs. 3, 9, and 10.

The parameters J_1, J_2, J_3, and J were chosen such that the best overall agreement for all three experimental quantities is obtained. Although some systematic deviations remain, these results, show that it is, in principle, possible to explain the behavior of the specific heat, susceptibility, and magnetization simultaneously, on the basis of the set of assumptions (i)–(iv) given above. Evidently, a better agreement for the magnetization and susceptibility can be obtained if we use instead of the average magnetic moment, the slightly different magnetic moments as obtained from the magnetization and susceptibility experiments.

The agreement of the prediction based on the ENNPA with the data appears to be worse for the higher concentrations. A similar effect was observed for CMA[1] and it confirms the conclusion that the ENNPA is probably not a suitable approximation for higher concentrations, because the role of large clusters is not taken into account.

In the preceding section we obtained a relation between the interaction parameters and the Curie-Weiss temperature [Eq. (3)]. Writing J_1, J_2, and and J_3 separately in this equation, we obtain

$$\Theta = -(x/k_B)(16J_1 + 7.9J_2 + 2J_3 + 8.9J) . \tag{9}$$

Inserting the interaction parameters obtained from the ENNPA, we obtain $\Theta = -2126x$ K. This result agrees fairly well with the experimental behavior, $\Theta = -(2000 \pm 200)x$ K (see also Fig. 8).

As an additional check on the approximation we performed experiments on the specific heat in an external field. Figure 9 shows a typical result together with the prediction from the ENNPA, assuming the same set of interaction parameters as above. The agreement is rather satisfactory and confirms the applicability of the approximation.

One may conjecture that the ENNPA could be im-

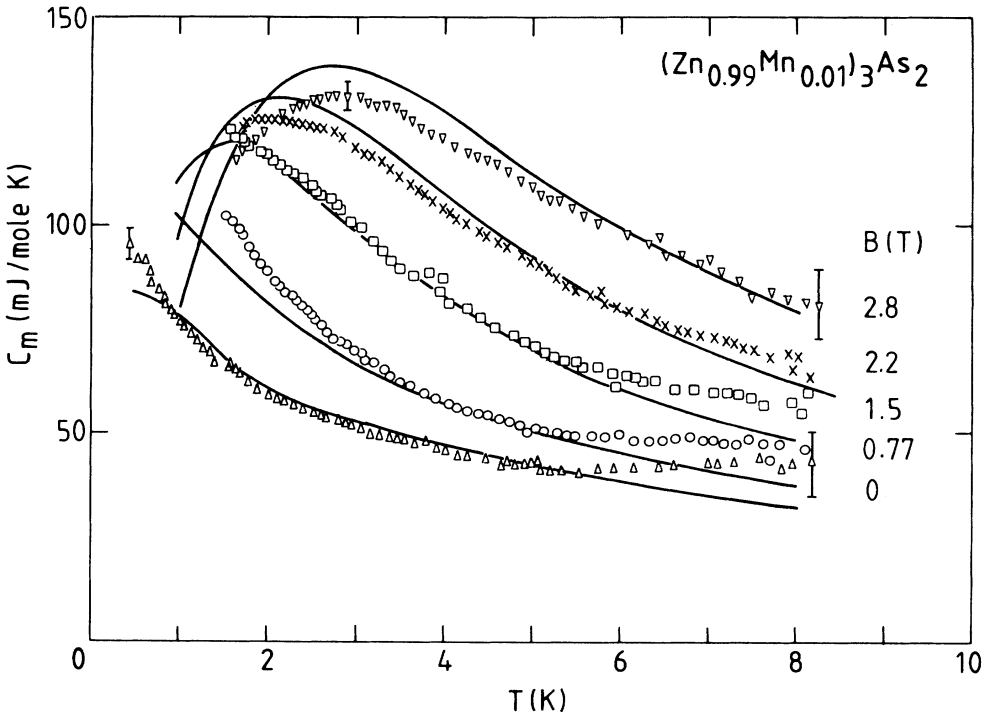

FIG. 9. Magnetic field dependence of the magnetic specific heat of ZMA. The solid curves are obtained from the ENNPA using the same parameters as in Fig. 3.

proved for the magnetization and susceptibility by combining it with a mean field approximation, to account for the average interaction of a spin with the other spins not belonging to the pair or triple. The interactions of the spins outside shell $\bar{\nu}$ with a pair or a triple are included in an internal magnetic field and the Hamiltonians [Eqs. (4) and (5)] now read

$$\mathcal{H}_\nu^P = -2J_\nu \mathbf{S}_i \cdot \mathbf{S}_\nu - g\mu_B B_{\text{eff}}^z (S_i^z + S_\nu^z) , \tag{10}$$

$$\mathcal{H}_\nu^T = -2J_\nu (\mathbf{S}_i \cdot \mathbf{S}_{\nu,1} + \mathbf{S}_i \cdot \mathbf{S}_{\nu,2}) - g\mu_B B_{\text{eff}}^z (S_i^z + S_{\nu,1}^z + S_{\nu,2}^z) , \tag{11}$$

where $B_{\text{eff}}^z = B_{\text{ext}}^z + B_{\text{int}}^z$, and ν still runs from 1 up to $\bar{\nu}$.

The internal field B_{int}^z is given by

$$B_{\text{int}}^z = \frac{2}{g\mu_B} x \langle S_{\text{av}}^z \rangle J \sum_{\nu=\bar{\nu}+1}^{\infty} N_\nu / R_\nu^{4.5} . \tag{12}$$

$\langle S_{\text{av}}^z \rangle$ is the weighted average of $S_\nu^z \rangle$ of pairs and triplets:

$$\langle S_{\text{av}}^z \rangle = \sum_{\nu=1}^{\bar{\nu}} [P_\nu^P(x) \langle (S_\nu^z)^P \rangle / 2 + P_\nu^T(x) \langle (S_\nu^z)^T \rangle / 3] . \tag{13}$$

Equations (10)–(13) form a self-consistent set with B_{int}^z and $\langle S_{\text{av}}^z \rangle$ as a solution. In Figs. 10 and 11 the results for the magnetization and the susceptibility are given. The zero-field specific-heat results are identical to the results of the bare ENNPA ($\langle S_{\text{av}}^z \rangle = 0$).

The results generally confirm the conjecture, that implementation of a mean field term will improve the theoretical description of the thermodynamic properties. This is particularly true for the magnetization results, since the "corrections" due to the mean field are small for the specific heat and susceptibility because in those cases $\langle S_{\text{av}}^z \rangle$ is rather small. It should be noted that no

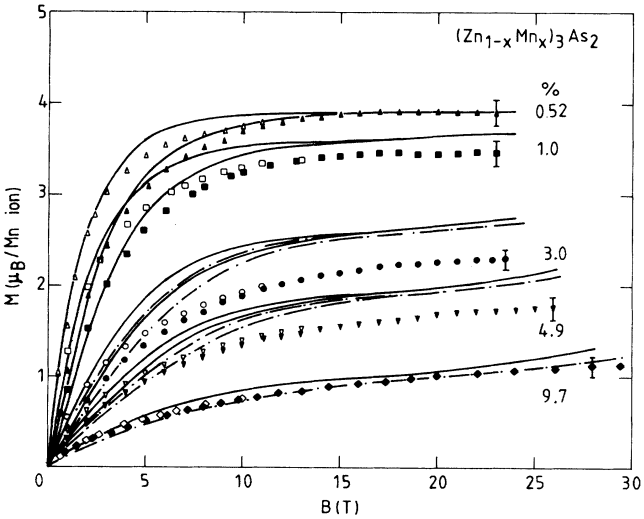

FIG. 10. High-field magnetization M of ZMA. Open and closed symbols represent data collected at $T=2$ K and $T=4.2$ K, respectively. The solid curves represent the calculations with the ENNPA using the same parameters as in Fig. 3. The dashed-dotted curves represent the calculations with the ENNPA extended with a mean-field approximation.

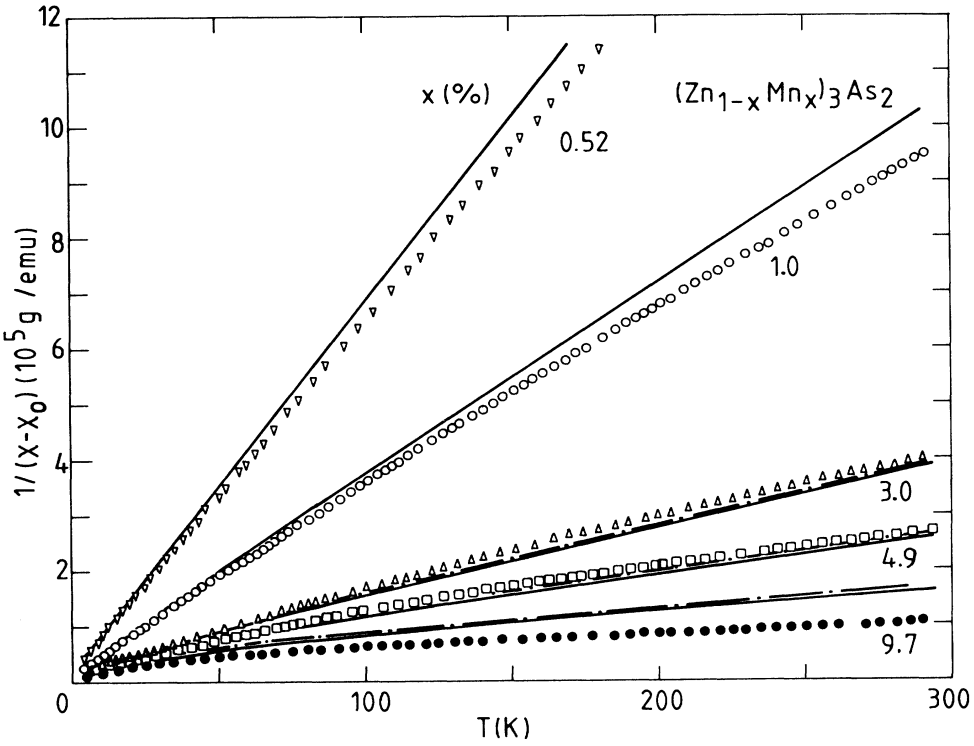

FIG. 11. Inverse high-temperature susceptibility of ZMA. The solid lines are results of the calculations similar to those in Fig. 3. The dashed-dotted lines reflect the inclusion of a mean-field term, as in Fig. 9.

additional fitting parameters have been used. All calculations have been made with an identical set of exchange parameters.

The introduction of a mean-field term representing an antiferromagnetic exchange generally decreases the magnetization, as could be expected. With increasing concentration x, the effect of the inclusion of a mean-field term on the theoretical prediction becomes more obvious. In the present case it results in very good description of the data for the highest concentration ($x = 9.7\%$). The increasing influence of the mean-field term with x probably reflects the increasing average interaction energy in a more condensed array of magnetic ions.

IV. CONCLUDING REMARKS AND DISCUSSION

Although the theoretical results presented in foregoing sections seem to describe the observed behavior of C_m, M, and χ rather satisfactorily, some systematic deviations are still apparent. It is hard to conclude whether these deviations arise from the inadequacy of the model representing the various interactions itself or result from the simplicity of the extended nearest-neighbor pair approximation. The latter argument will certainly hold for higher concentrations. Nevertheless we feel that the present experiments have yielded reliable data on the range and magnitude of the major interactions as well as the statistical distribution and local moment of the Mn ions. At this point we would like to emphasize once more that our model is designed to describe the available data simultaneously. In earlier publications we have demonstrated that this approach, in principle also yields consistent results for the available magnetic and thermal data of more canonical DMS like (Cd,Mn)Te,[8,9] (Hg,Mn)Te,[8] and (Zn,Mn)Se,[10] including the steps in the magnetization. In order to describe C_m as well as χ and M, however, one has to implement the (small) interactions between further neighboring Mn^{2+} ions since specifically the low-temperature contribution to the zero-field C_m probes mainly that part of the interaction range. The relative importance of these long-range terms depends of course on the radial dependence of J. It has been shown recently[9,10] that considerable differences in that respect seem to exist between the wide gap materials like (Cd,Mn)Te [$J(R) \sim R^{-6.8}$] and the present compound [$J(R) \sim R^{-4.5}$]. Evidently an interpretation with a model which takes into account a few neighbors only, is expected to be more adequate in a system with sharply decreasing interaction strength, like (Cd,Mn)Te, than in systems with a longer interaction range. However, even for (Cd,Mn)Te, a cluster model as used by Larson *et al.*,[11] for instance, to explain the steps in the magnetization, does not reproduce the low-temperature specific heat in that system. For $(Zn_{1-x}Mn_x)_3As_2$ the influence of the long-range term is illustrated in Fig. 3.

Let us recall that the main reason for the investigation of ZMA was to obtain additional information on the origin of the magnetic long-range interaction in DMS. We will therefore focus on this issue in the remainder of this section. With respect to the spin-glass transition, we refer to the general conclusions formulated in Ref. 1.

For ZMA, the role of the Ruderman-Kittel-Kasuya-Yosida (RKKY) oscillatory type of exchange[12] can be

ruled out because the free carrier concentration in ZMA is only 10^{16} cm^{-3}.

As quoted in the Introduction, we have two other possible alternatives for the physical origin of the long-range interaction; the Bloembergen-Rowland mechanism,[13] which was calculated by Lewiner and Bastard for a narrow-gap semiconductor,[14] and the superexchange mechanism.[15,16] We first will comment on the Bloembergen-Rowland mechanism. According to this mechanism, the interaction for an wide-gap semiconductor can be written as

$$J(R)\sim f(R)\exp(-k_0R)\ . \tag{14}$$

$k_0=\hbar^{-1}(2m^*\varepsilon_0)^{1/2}$, where m^* is the sum of the electron and hole masses. For a vanishingly small gap ε_0 (narrow-gap semiconductor) the exponential decay is no longer present and the long-range interaction is only determined by the radial dependence $f(R)$. For the wide-gap semiconductor ZMA we would expect an additional exponential decrease $\exp(-1.29R_v)$, where R_v is in units of the nearest-neighbor distance in ZMA ($\varepsilon_0=0.99$ eV, $m_e=0.04m_0$, and $m_h=0.7m_0$, m_0 is the electron rest mass[17]). Combined with $f(R)$, which for an wide-gap semiconductor is theoretically estimated as R^{-n}, $4<n<5$,[14] the interaction can be written as

$$J(R_v)\sim R_v^{-n}[\exp(-1.29R_v)]\ ,\quad 4<n<5\ . \tag{15}$$

In Table V the range of this interaction ($n=4$) is compared with the range experimentally found for ZMA. It is obvious that the predicted interaction is of much shorter range than experimentally observed. It is therefore not very likely that the long-range interaction is due to the Bloembergen-Rowland mechanism.

This conclusion is corroborated by the fact that T_f decreases with increasing Cd concentration in a series of quaternary compounds $(Cd_{1-y-x}Zn_yMn_x)_3As_2$ with $x=10\%$ as shown in Fig. 12. The substitution of Cd in Zn_3As_2 has been shown to decrease the gap. The decrease of T_f therefore is in marked disagreement with the expectation based on the Bloembergen-Rowland mechanism. This conclusion confirms the theoretical results of Larson *et al.*[16] who analyzes the hierarchy of exchange mechanisms in II-VI DMS. The Bloembergen-Rowland mechanism was found to be of minor importance and superexchange was shown to be dominant, at least at nearest- and next-nearest-neighbor distances.

Generally, the interaction resulting from superexchange is based on the notion of the admixture of the p wave function representing the completely filled anion

TABLE V. Comparison of the range of the exchange interaction for two different radial dependences of $J(R)$.

R_v	$J(R)\sim(1/R_v^4)[\exp(-1.29R_v)]$	$J(R)\sim 1/R_v^{4.5}$
1	1	1
$\sqrt{2}$	1.5×10^{-1}	2.1×10^{-1}
$\sqrt{5}$	8.1×10^{-3}	2.7×10^{-2}
$\sqrt{10}$	6.1×10^{-4}	5.6×10^{-3}
$\sqrt{15}$	1.1×10^{-4}	2.3×10^{-3}
$\sqrt{20}$	2.8×10^{-5}	1.2×10^{-3}

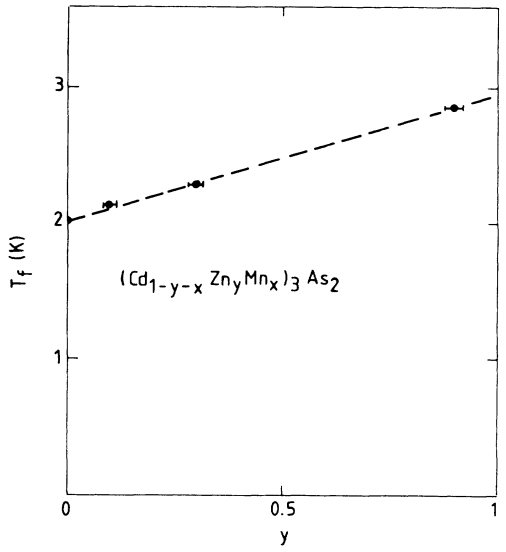

FIG. 12. Freezing temperature T_f as a function of the Zn concentration at constant ($x=10$ at. %) Mn concentration in $(Cd_{1-y-x}Zn_yMn_x)_3As_2$.

band to the $3d^5$ states of Mn^{2+}.[15] This interaction is antiferromagnetic and becomes long range if the d states of Mn^{2+} are hybridized with the states close to the top of the valence band. It is predicted that if the d states approach the top of the band the interaction becomes more long range, but the absolute magnitude of the interaction decreases. Comparing the results of ZMA and CMA we observe that for ZMA the range of the interaction has decreased, while the magnitude of the interaction has increased with respect to CMA. Preliminary results of photoelectron spectroscopy measurements[18] on CMA indicate strongly hybridized d states of Mn^{2+} close to top of the valence band. Based on the above argument we would expect the d states of Mn^{2+} in ZMA less close to the top of the valence band. The investigations to check this prediction are currently undertaken.

Also the reduction of the magnetic moment with respect to the free electron value in both CMA and ZMA can be understood on the basis of a strong hybridization of the d states of Mn^{2+}. The coefficient b, usually called the covalency factor, describes the amount of p-d mixing. From $\Delta S=b^2S\simeq0.3$ we find $b^2\simeq0.12$, which is larger than for other DMS, i.e., CdMnTe.[19]

Recently also for other DMS, belonging to the II-VI group, evidence has been obtained that superexchange is the dominant exchange interaction.[16,19] Spałek *et al.*[19] related the systematic variation of the nearest-neighbor exchange in Zn and Cd compounds of the II-VI group to the superexchange integral, which depends on the bonding angle θ of $\angle$Mn–X–Mn (X is the anion) as[20]

$$J(\theta)=J(\pi/2)+[J(\pi)=J(\pi/2)]\cos^2\theta\ , \tag{16}$$

where $J(\pi/2)$ and $J(\pi)$ are the superexchange integrals for $\theta=90°$ and 180°, respectively. $J(\pi/2)\simeq2J(\pi)$ (Ref. 21) and, as both these integrals are antiferromagnetic, $J(\theta)$ is antiferromagnetic.

Following a similar line as Spałek *et al.*,[19] the observed increase of the antiferromagnetic nearest-neighbor interaction from $J_1/k_B = -30$ K in CMA to $J_1/k_B = -100$ K in ZMA would be caused by a variation of the bonding angle Mn-As-Mn in ZMA compared with CMA. Since $\theta < 90°$ in the pure compounds this would, according to Eq. (16), lead to $\theta(\text{ZMA}) > \theta(\text{CMA})$. Although no detailed information is available on this subject, this variation in θ is, however, not in agreement with intuitive arguments based on the radii of the ions.[19] Also the ration between the magnitude of the nearest-neighbor interaction of both compounds is not in agreement with Eq. (16), as this equation predicts a maximum ratio of 2 in the entire θ region between 0° and 90°.

ACKNOWLEDGMENTS

The authors wish to acknowledge the stimulating discussions with R. Gałązka and J. A. Mydosh. Thanks are due to A. T. A. M. de Waele for the very low temperature ac susceptibility measurements and to C. van der Steen and P. A. M. Nouwens for their technical assistance and preparation of the samples. We also thank S. Takeyama, N. Miura, K. Koga and H. Yasuoka for their continuous encouragements.

---

*On leave from Physics Department, Nanjing University, Nanjing, China.

[1]C. J. M. Denissen, H. Nishihara, J. C. v. Gool, and W. J. M. de Jonge, Phys. Rev. B **33**, 7637 (1986).

[2]A. Pietrazko and K. Lukaszewics, Phys. Status Solidi A **18**, 723 (1979); R. J. Wagner, E. D. Palik, and E. M. Swiggard, Proceedings of the Conference on the Physics of Semimetals, Narrow-Gap Semiconductors (Dallas) [J. Phys. Chem. Solids Suppl. **1**, 471 (1970)]; E. K. Arushanov, Prog. Cryst. Growth Charact. **3**, 211 (1981).

[3]J. Souletie, J. Phys. (Paris) Colloq. **39**, C2-3 (1978); J. L. Tholence and R. Tournier, J. Phys. (Paris) Colloq. **35**, C4-229 (1974).

[4]M. Escorne, A. Mauger, R. Triboulet, and J. L. Tholence, Physica **107B**, 309 (1981).

[5]D. L. Martin, Phys. Rev. B **20**, 368 (1979).

[6]J. S. Smart, *Effective field theories of Magnetism* (Saunders, Philadelphia, 1966).

[7]K. Matho, J. Low Temp. Phys. **35**, 165 (1979).

[8]C. J. M. Denissen and W. J. M. de Jonge, Solid State Commun. **39**, 503 (1986).

[9]W. J. M. de Jonge, A. Twardowski, and C. J. M. Denissen in, *Diluted Magnetic (Semimagnet) Semiconductors*, Vol. 89 of *Material Research Society Symposium Proceedings*, edited by J. K. Furdyna, R. L. Aggarwal, and S. von Moluar (MRS, University Park, PA, 1987).

[10]A. Twardowski, C. J. M. Denissen, W. J. M. de Jonge, A. T. A. M. de Waele, M. Demianiuk, and R. Triboulet, Solid State Commun. **59**, 199 (1986); A. Twardowski, H. J. M. Swagten, W. J. M. de Jonge, and M. Demianiuk (unpublished).

[11]B. E. Larson, K. C. Hass, and R. L. Aggarwal, Phys. Rev. B **33**, 1789 (1986).

[12]M. A. Ruderman and C. Kittel, Phys. Rev. **96**, 99 (1954); K. Yosida, Phys. Rev. **106**, 893 (1957); T. Kasuya, Prog. Theor. Phys. **16**, 45 (1956).

[13]N. Bloembergen and T. J. Rowland, Phys. Rev. **97**, 1679 (1955).

[14]C. Lewiner and G. Bastard, J. Phys. C **13**, 2347 (1980); C. Lewiner, J. A. Gaj, and G. Bastard, J. Phys. (Paris) Colloq. **41**, C5-289 (1980).

[15]W. Geertsma, C. Haas, G. A. Sawatzky, and G. Vertogen, Physica **86-88A**, 1039 (1977); G. A. Sawatzky, W. Geertsma, and C. Haas, J. Magn. Magn. Mater. **3**, 37 (1976); C. E. T. Concalves da Silva and L. Falicov, J. Phys. C **5**, 63 (1973); W. Geertsma, Ph.D. thesis, University of Groningen, 1979 (unpublished).

[16]B. E. Larson, K. C. Hass, H. Ehrenreich, and A. E. Carlsson, Solid State Commun. **56**, 347 (1985).

[17]Landolt-Bornstein, Vol. 17e, edited by O. Madelung (Springer-Verlag, Berlin, 1983).

[18]G. A. Sawatzky (private communication).

[19]J. Spałek, A. Lewicky, Z. Tarnawski, J. K. Furdyna, R. R. Gałązka, and Z. Obuszko, Phys. Rev. B **33**, 3407 (1986).

[20]C. Boekema, F. van der Woude, and G. A. Sawatzky, Int. J. Magn. **3**, 341 (1972).

[21]J. Owen and J. H. M. Thornley, Rep. Prog. Phys. **29**, 675 (1966).